Acta Crystallographica Section B
Structural Science
ISSN 0108-7681

Structural characterization of $SmMn_2GeO_7$ single microcrystals by electron microscopy

E. A. Juarez-Arellano,[a,b]* J. M. Ochoa,[a] L. Bucio,[a] J. Reyes-Gasga[a] and E. Orozco[a]

[a]Instituto de Física, UNAM Apartado Postal 20-364, 01000 México DF, Mexico, and [b]Universidad de Guadalajara, Centro Universitario de la Ciénega, Apartado Postal 106, Km 33 carretera Ocotlán-Tototlán, Ocotlán Jalisco, Mexico

Correspondence e-mail: erickj@fisica.unam.mx

Received 31 July 2004
Accepted 28 October 2004

Single microcrystals of the new compound samarium dimanganese germanium oxide, $SmMn_2GeO_7$, were grown using the flux method in a double spherical mirror furnace (DSMF). The micrometric crystals were observed and chemically analysed with scanning electron microscopy (SEM) and X-ray energy dispersive spectroscopy (EDX). The structural characterization and chemical analysis of these crystals were also carried out using transmission electron microscopy (TEM) and high-resolution transmission electron microscopy (HRTEM), together with electron-energy-loss spectroscopy (EELS). We found that the new quaternary compound crystallizes in the orthorhombic system with the point group *mmm* (D_{2h}), space group *Immm* (No. 71) and cell parameters a = 8.30 (10), b = 8.18 (10), c = 8.22 (10) Å and V = 558.76 Å^3.

1. Introduction

In recent years, rare-earth manganates have received much attention because of their extraordinary physical properties (optical emission, high magneto resistance) and technical applications (cathode materials in solid oxide fuel cells, catalysts in the oxidation of hydrocarbons or carbon monoxide). These properties not only attract interest in the mixed oxidation states of manganese, but have also opened up the possibility of rare-earth manganates as reading heads for magnetic sensors (Kim *et al.*, 2002; Vijaya Sarathy *et al.*, 2001; Duk-Young & Payne, 1999). The rare-earth manganates also exhibit other interesting phenomena, such as the transition from paramagnetic at room temperature to ferromagnetic at 200–280 K. Alternatively, the phase separation that occurs from a pure monophasic oxide into two or more phases in certain transition-metal oxides after a threshold temperature (Pattison *et al.*, 2000; Rao *et al.*, 2003).

Most of these rare-earth manganates contain a transition metal with covalent elements such as silicon or germanium; only a few quaternary compounds are reported in the literature. Among the reported ones we found $GdMnGe_2O_7$, $EuMnGe_2O_7$, $CeMn_2Ge_4O_{12}$ and $PrMnGeO_5$ (Taviot-Guého *et al.*, 1999; Juarez-Arellano *et al.*, 2001; Taviot-Guého *et al.*, 1995). In order to explore these quaternary germanates, we have synthesized the $SmMn_2GeO_7$ compound in a DSMF in combination with a variation of the flux-synthesis method (Juarez-Arellano, Rosales, Gamboa-Espinosa *et al.*, 2004). Unfortunately, not enough compound was found to perform the crystal structure characterization by X-ray powder diffraction and the crystal size was not large enough for X-ray single-crystal diffraction analysis. We are working on synthesizing larger crystals and/or a more suitable material for

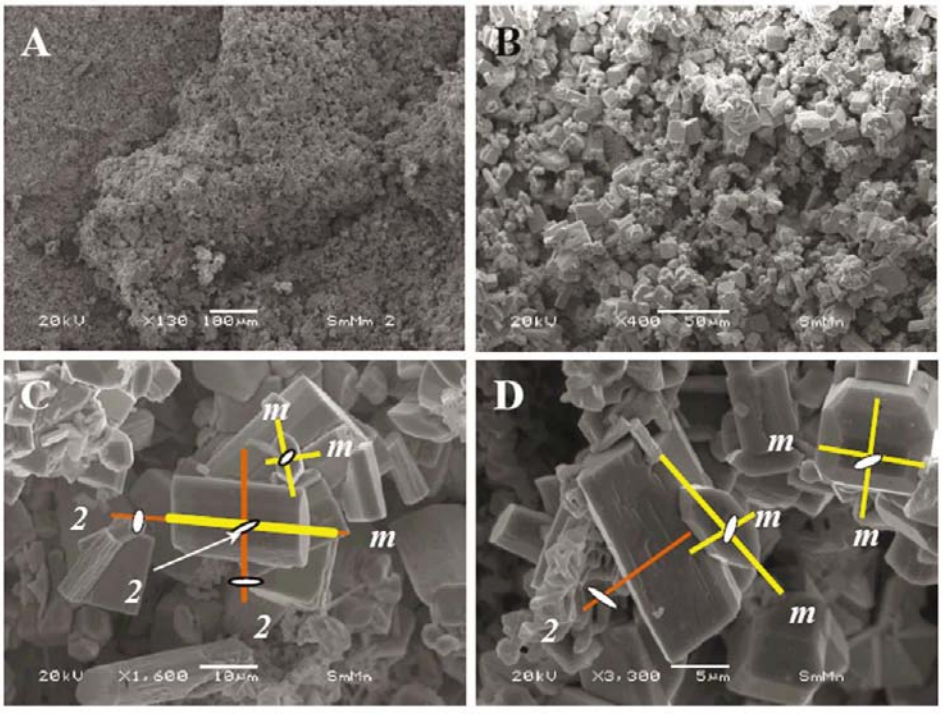

Figure 1
SEM images of the synthesized micro-crystals for the Sm–Mn–Ge–O system. (*a*) General view; (*b*) a close-up; (*c*) and (*d*) crystal morphology characteristics. Note the crystal size and the symmetry elements that they present.

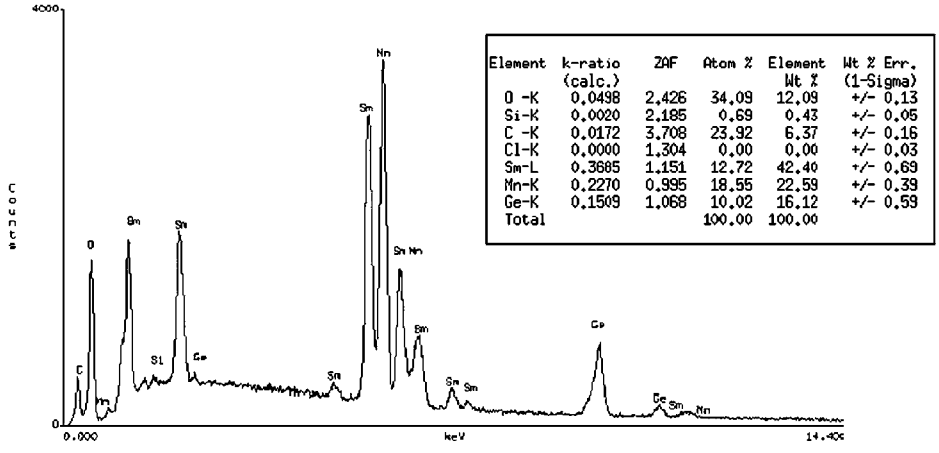

Element	k-ratio (calc.)	ZAF	Atom %	Element Wt %	Wt % Err. (1-Sigma)
O -K	0.0498	2.426	34.09	12.09	+/- 0.13
Si-K	0.0020	2.185	0.69	0.43	+/- 0.05
C -K	0.0172	3.708	23.92	6.37	+/- 0.16
Cl-K	0.0000	1.304	0.00	0.00	+/- 0.03
Sm-L	0.3685	1.151	12.72	42.40	+/- 0.69
Mn-K	0.2270	0.995	18.55	22.59	+/- 0.39
Ge-K	0.1509	1.068	10.02	16.12	+/- 0.59
Total			100.00	100.00	

Figure 2
Semi-quantitative EDX spectrum from the crystals. The inset shows the main percentages for the elements shown in the spectrum.

analysis of this compound by X-ray powder diffraction. However, here we want to encourage the use of electron microscopy to perform a structural and chemical characterization.

2. Experimental

The $SmMn_2GeO_7$ compound was prepared by modifying the method reported by Taviot-Guého *et al.* (1995). For the synthesis, MnO_2, GeO_2 and $SmCl_3$ were mixed in stoichiometric proportions and heated at 323 K in air for 3 d. Afterwards, the sample was placed inside of an evacuated quartz tube maintained at 573 K. The quartz tube was placed inside a reflective furnace (Lara *et al.*, 1991) and the chemical transport reaction was carried out at 1073 K for 12 h (Schäfer, 1964; Gruehn & Schweizer, 1983). After the thermal treatment many microcrystals were formed on the wall of the quartz tube, showing a perfect crystalline appearance. Hereafter we will name these microcrystals 'crystals' for simplicity. The resulting product of the reaction was stirred using ethanol to dissolve the $MnCl_2$ sub-product. The crystals were studied with SEM and EDX as obtained.

In order to perform the TEM analysis, the crystals obtained were taken from the tube of quartz and millied in an agate mortar. The resulting powder was collected and supported on Cu grids that had been previously covered with a plastic film.

For SEM and EDX analysis, a Jeol SEM 5200 microscope with a NORAN-EDX instrument was used. TEM observations were carried out with three different microscopes. For conventional microscopy an analytical electron microscope Jeol STEM 100-CX was used. High-resolution images, Z-contrast and electron-energy-loss spectra (EELS), and convergent-beam diffraction patterns were obtained with Jeol 4000-EX and Jeol-FEG-2010-EX microscopes.

3. Results and discussion

A general view of the crystals obtained is shown in Fig. 1. The crystals are very well formed and their size is in the range 1–10 µm. Therefore, the crystallographic study began with the analysis of the crystal shape observed in SEM images.

In Figs. 1(*c*) and (*d*) a typical crystal morphology is clearly exhibited. The procedure followed in order to assign the crystal's symbolic point-group notation, on the basis of the symmetry operations that they present, has been reported elsewhere (Klein, 1989). We started by looking for four threefold axes (without any success), an *n*-fold axes (see Figs.

Table 1
Lattice parameters for $EuMnGe_2O_7$, $GdMnGe_2O_7$ and $SmMn_2GeO_7$.

Lattice parameters	$EuMnGe_2O_7$	$GdMnGe_2O_7$	$SmMn_2GeO_7$	$SmMn_2GeO_7$
a (Å)	4.6 (2)	4.735 (1)	8.30 (10)	4.15†
b (Å)	8.5 (4)	7.839 (2)	8.18 (10)	8.18
c (Å)	12.7 (6)	13.500 (3)	8.22 (10)	12.18‡
V (Å^3)	495.6	501.09	558.76	413.47
Space group	$A222$ (No. 21)	$A222$ (No. 21)	$Immm$ (No. 71)	$Immm$ (No. 71)

† Half of the real 'a' lattice parameter value. ‡ One and a half of the real 'c' lattice parameter value.

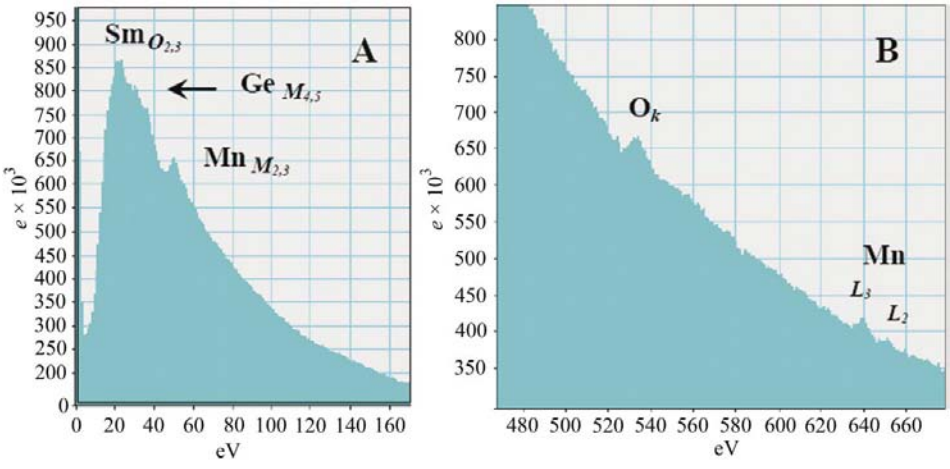

Figure 3
EELS spectrum from the crystals. The major and minor edges from Mn and Sm are resolved.

1c–*d*), twofold axes perpendicular to the *n*-fold axis, with mirrors perpendicular to the *n*-fold axis (yes, Figs. 1*c*–*d*). From here only four point groups from a possible 32 can be assigned: *mmm*, 4/*mmm*, $\bar{6}m2$ and 6/*mmm*. From Fig. 1, it is clear that no three-, four- or sixfold axes exist. Therefore, we concluded that the crystalline system with the point group *mmm* (D_{2h}), which has three twofold axes which are mutually perpendicular and perpendicular to a mirror plane, is the correct one. In Figs. 1(*c*) and (*d*) the existence of these three twofold axes and the mirror planes are clearly observed, confirming the point group previously mentioned.

A semi-quantitative EDX spectrum from the crystal is shown in Fig. 2. This spectrum indicates the presence of germanium, samarium (manganese) and oxygen in the crystals. The reason for the parenthesis in the element Mn is on account of the energy values for Sm peaks [L_α (5.636 KeV) and L_β (6.587 KeV)], Mn peaks [K_α (5.895 KeV) and K_β (6.492 KeV)] and the EDX energy resolution (130 eV approximately), L_β of Sm and K_β of Mn are overlapping.

The table of percentages inserted in Fig. 2 therefore indicates an approximate chemical formula for the new compound, which is very close to $SmMn_2GeO_7$. Owing to the overlapping of peaks, the chemical analysis was also carried out with EELS in TEM, which easily resolved the overlap. These spectra are shown in Fig. 3, and the resulting analysis was again close to the formula $SmMn_2GeO_7$. The peak of carbon observed in the EDX spectra shown in Fig. 2 was produced by the graphite film that was used to cover the sample for its SEM analysis. Due to the crystals being synthesized in a sealed quartz tube, some additional subproduct elements were detected.

One particle of the new compound is observed in bright and dark field images in Fig. 4, where some structural defects can be seen.

A stereogram of the electron diffraction patterns was obtained from the crystals (Fig. 5) and, based on this stereogram, the reciprocal space of the crystal structure was built to obtain a global view and improve the interpretation of the images (Fig. 6).

The analysis of the stereogram and the three-dimensional reciprocal space structure indicates that the compound crystallizes in the orthorhombic system with cell parameters a = 8.3, b = 8.18, c = 8.22 Å and V = 558.09 Å^3. Moreover, assuming that the point group is *mmm* (D_{2h}), we looked for an isostructural compound in the Inorganic Crystal Structure Database (2003), without any success. Therefore, in order to determine the space group, we analyzed the (*hkl*) Bragg reflections in the electron diffraction patterns to identify any systematic extinction conditions.

Electron diffraction patterns along the directions [001], [010], [100] and [$\bar{1}$10] are shown in Fig. 7. Analysis of the first three diffraction patterns shows the existence of the following systematic extinction conditions 0*kl*: $k + l$; *h*0*l*: $h + l$; *hk*0: $h + k$; *h*00: *h*; 0*k*0; *k* and 00*l*. This information, with the orthorhombic cell as a reference, indicates eight space groups: *Pnnn* (No. 48), *I*222 (No. 23), $I2_12_12_1$ (No. 24), *I*2*mm* (No. 44), *Immm* (No. 71), *F*222 (No. 22), *Fmm*2 (No. 41) and *Fmmm* (No. 69). If the point group *mmm* (D_{2h}) is used, the possible space groups are reduced from eight to three: *Pnnn* (No. 48),

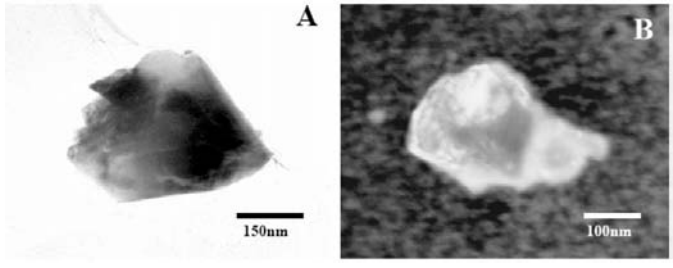

Figure 4
(*a*) TEM bright-field and (*b*) dark-field images of a powder particle from the crystals shown in Fig. 1.

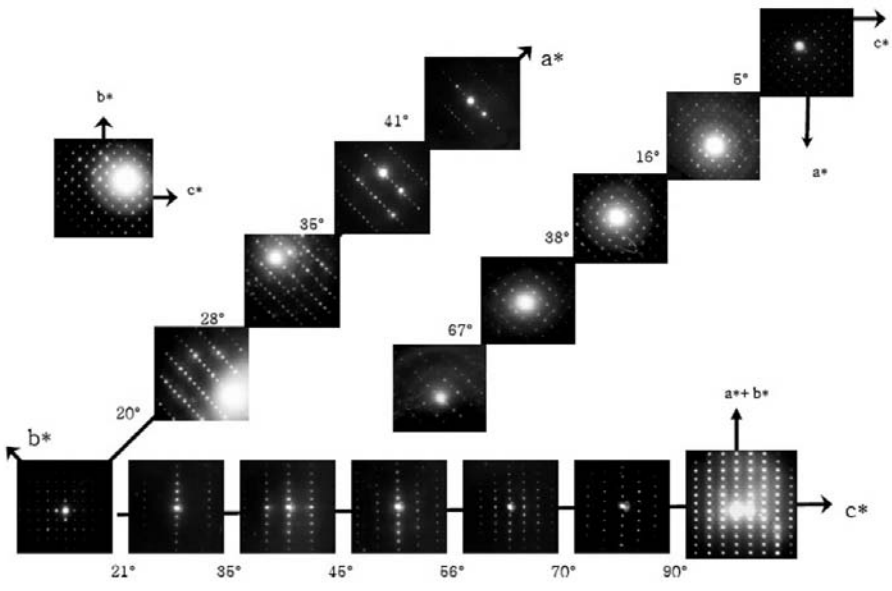

Figure 5
Electron diffraction pattern from the crystals.

material crystallizes in the orthorhombic system with the space group *Immm* (No. 71).

A *Z*-contrast image taken along the [$\bar{1}$10] direction is shown in Fig. 8. It is well known that contrast for this type of image is carried out taking into account the difference in atomic number of the elements that constitute the sample. Therefore, the element of the brightest lines may correspond to Sm (the heaviest element scatters more intensity on the annular dark field detector than the lighter ones, *Z* Sm = 62, *Z* Ge = 32 and *Z* Mn = 25), suggesting that the new compound crystallizes in a laminar structure that is related to the structures of $EuMnGe_2O_7$ and $GdMnGe_2O_7$ (Juarez-Arellano *et al.*, 2001).

Table 1 shows the lattice parameters for $EuMnGe_2O_7$, $GdMnGe_2O_7$ and $SmMn_2GeO_7$. In this table it can also be seen that the lattice parameters of $SmMn_2GeO_7$ could be sub-multiples of the lattice parameters of the reported compounds.

HREM images of $SmMn_2GeO_7$ crystals along different directions are shown in Fig. 9 as an example of the type of

Immm (No. 71) and *Fmmm* (No. 69). From Fig. 7(*d*) an extra systematic condition can be seen, *hkl*: $h + k + l$, which is generated for the body-centred lattice cell (I). This analysis is corroborated with the three-dimensional reciprocal space model (Fig. 6). Therefore, all the results indicated that this

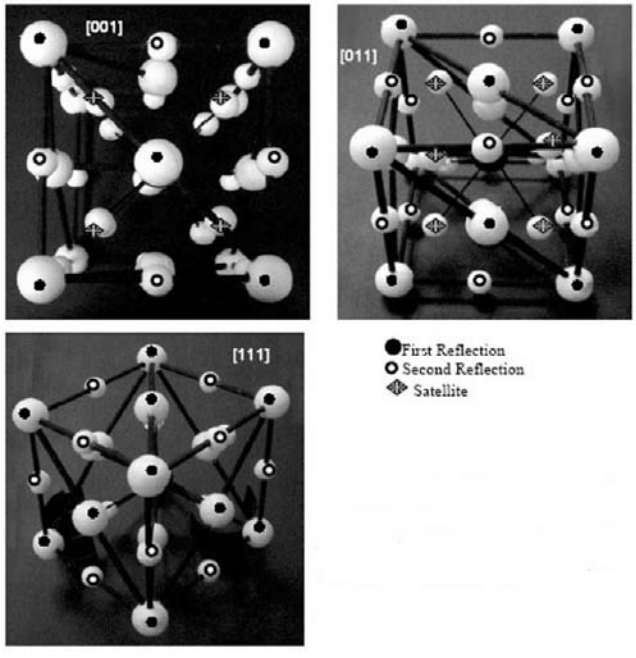

Figure 6
Reciprocal space structure of the crystals modelled according to the electron diffraction pattern shown in Fig. 5. Note the existence of satellite reflections in this structure.

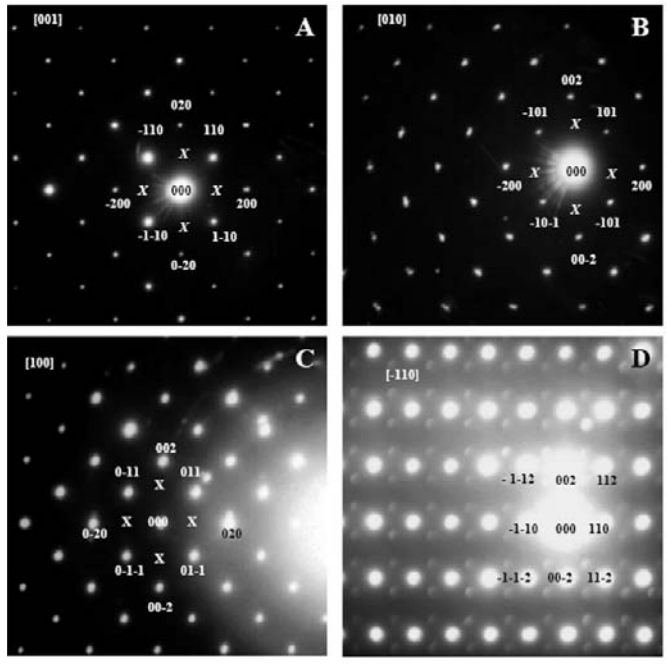

Figure 7
Main electron diffraction patterns of the crystals: (*a*) [001], (*b*) [010], (*c*) [100] and (*d*) [$\bar{1}$10]. Their indexation was carried out according to the reciprocal space structure shown in Fig. 6. 'X' indicates the systematic extinctions. Note the existence of satellite reflections in (*d*).

contrast observed in this mode of operation. These images are related to the diffraction patterns shown in Fig. 7. The images along the [001] axis zone direction with two different defocus values are shown in Figs. 9(*a*) and (*b*), while the [100] and [$\bar{1}$10] directions are presented in Figs. 9(*a*)–(*d*), respectively. The interpretation of these HREM images is only possible when the exact positions of the atoms in the unit cell of the crystal are well known (Wan *et al.*, 2003; Morniroli & Steeds, 1992). In our case this is not the situation and a computer image simulation cannot carry on. Note that Fig. 9(*d*) was taken in the same direction as the *Z*-contrast image shown in Fig. 8, and in both images we can see the same layers and periodicity. An enlargement of Fig. 9(*d*) is shown as an inset.

It is also important to notice the existence of satellites. For example, in Fig. 6(*d*) the satellites are shown surrounding the reflections of the main diffraction pattern. These satellites were also observed in other diffraction patterns of the stereogram in Fig. 5, giving place to the reciprocal space structure shown in Fig. 6. The electron beam energy modifies the observation of these satellites in a certain way, as seen in Fig. 10. In this figure the same diffraction patterns taken with different electron microscopes are presented. The diffraction patterns with satellites (Figs. 10*a* and *c*) were easily observed with the electron microscope 100CX. However, when the material was analyzed with higher voltage electron microscopes (2010 FEG and 4000-EX) the interaction with the electron beam results in these satellites immediately disappearing (Figs. 10*b* and *d*). This behaviour indicates that the satellites could be produced by some type of vacancy or structure formed by light elements, such as oxygen. However, at the moment of interaction with the electron beam from high-voltage microscopes these structures are easily removed. This will be the topic of future work.

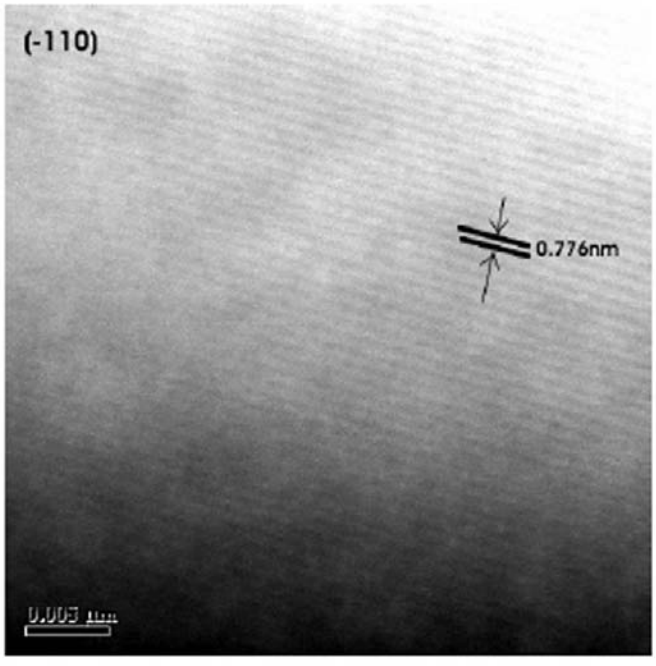

Figure 8
TEM *Z*-contrast image along the [$\bar{1}$10] direction. The bright lines indicate rows of Sm atoms.

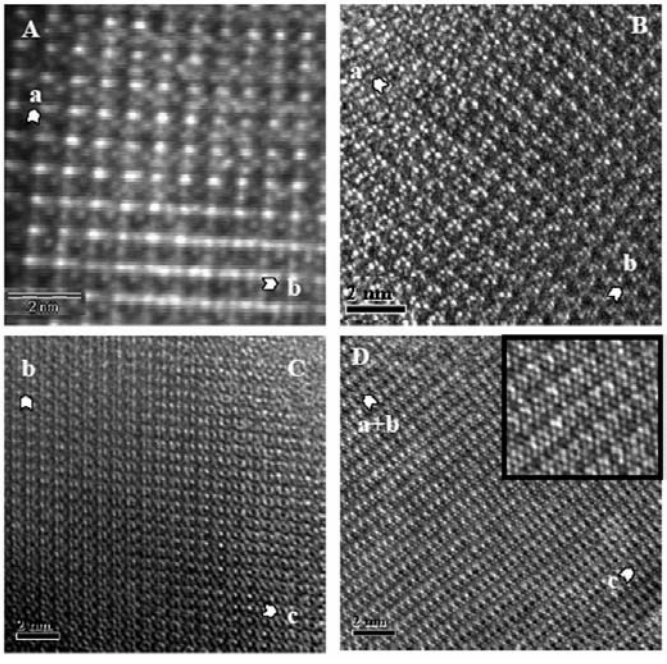

Figure 9
HREM images from the crystals along some of the electron diffraction patterns shown in Fig. 7. (*a*) [001]; (*b*) [001], but with different defocus value; (*c*) [100]; (*d*) [$\bar{1}$10]. The inset shows a higher magnification of an area in (*d*).

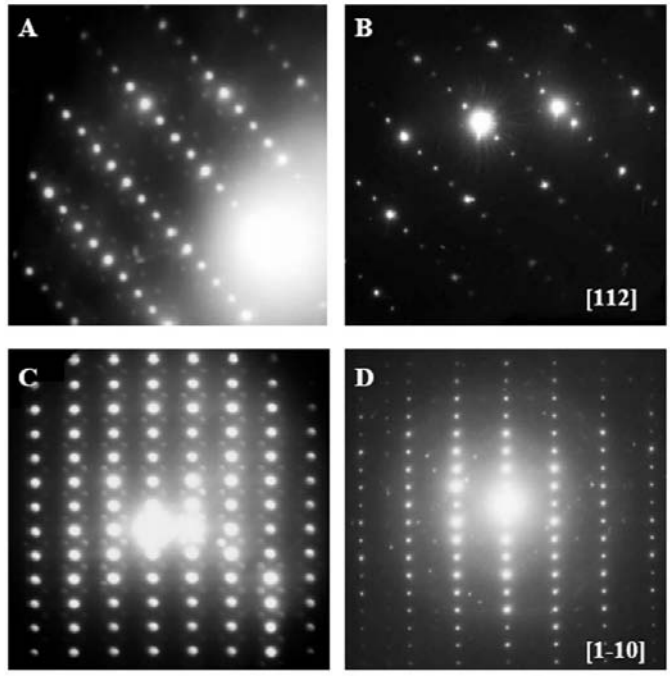

Figure 10
Electron diffraction patterns from the crystals obtained with different electron microscopes (*a* and *c*) with a 100 kV microscope while (*b* and *d*) with a 200 kV and 400 kV microscopes respectively. Note the existence of satellite reflections in (*a*) and (*c*), and their disappearance in (*b*) and (*d*).

In the study of the $ABGe_2O_7$ compounds (A = rare-earth elements; B = In, Fe, Mn) our group has synthesized the compounds AInGe$_2$O$_7$ (A = Fe, Y, Gd, Tb, Ho; Bucio *et al.*, 2001; Juarez-Arellano, Bucio, Moreno-Tovar *et al.*, 2002; Juarez-Arellano, Rosales, Bucio & Orozco, 2002; Juarez-Arellano *et al.*, 2003; Juarez-Arellano, Rosales, Oliver *et al.*, 2004). The main characteristic of these compounds is the existence of Ge_2O_7 diortho groups in the structure (Bucio *et al.*, 2003). In the new compound we reported, $SmMn_2GeO_7$, this diortho group could still be there, but rather than having a diortho group formed by two tetrahedra of germanium, it could have a diortho group formed by the union of a germanium and manganese tetrahedron ($MnGeO_7$).

4. Conclusions

We have performed the structural characterization of microcrystals of the compound $SmMn_2GeO_7$ by electron microscope. These crystals crystallize in the orthorhombic system with cell parameters a = 8.3, b = 8.18, c = 8.22 Å and V = 558.09 Å^3; point group *mmm* (D_{2h}) and space group *Immm* (No. 71).

The authors wish to express theirs thanks to D. Argott de Juarez, L. Rendon, A. Lara, J. Cañetas, P. Mexia, C. Magaña, C. Zorrilla, S. Tehuacanero, R. Hernández and G. Gamboa-Espinosa for technical help. They also thank Microscopy Central Laboratory (LCM-IFUNAM) and DGAPA-UNAM under projects PAPIIT-IN 113199, IN-104902, IN-120801 and IN-101003. One of the authors (E. A. Juarez-Arellano) acknowledges a fellowship from CONACyT.

References

Bucio, L., Pérez-Castro, L., Juarez-Arellano, E. A., Moreno-Tovar, R., Rosales, I. & Orozco, E. (2003). *Res. Adv. Chem. Mater.* **1**, 65–75.

Bucio, L., Ruvalcaba-Sil, J. L., Rosales, I., García-Robledo, J. & Orozco, E. (2001). *Z. Kristallogr.* **216**, 438–441.

Duk-Young, J. & Payne, D. A. (1999). *Bull. Korean Chem. Soc.* **20**, 824–826.

Gruehn, R. & Schweizer, H. (1983). *Angew. Chem.* **95**, 80–93.

Inorganic Crystal Structure Database ICSD Release (2003). National Institute of Standards & Technology, Gaithersburg. Fachinformationszentrum Karlsruhe.

Juarez-Arellano, E. A., Bucio, L., Hernandez, A. J., Camarillo, E., Carbonio, R. E. & Orozco, E. (2003). *J. Solid State Chem.* **170**, 418–423.

Juarez-Arellano, E. A., Bucio, L., Moreno-Tovar, R., García-Robledo, J. F. & Orozco, E. (2002). *Z. Kristallogr.* **217**, 201–204.

Juarez-Arellano, E. A., Gamboa-Espinosa, G. V., Lara, J. A., Bucio, L. & Orozco, E. (2001). *Latin Am. J. Metall. Mater.* **21**, 9–12.

Juarez-Arellano, E. A., Rosales, I., Bucio, L. & Orozco, E. (2002). *Acta Cryst.* C**58**, i135–i137.

Juarez-Arellano, E. A., Rosales, I., Gamboa-Espinosa, G. V., Lara, J. A., Bucio, L. & Orozco, E. (2004). *Cryst. Res. Technol.* **39**, 833–839.

Juarez-Arellano, E. A., Rosales, I., Oliver, A., Ruvalcaba, J. L., Carbonio, R. E., Bucio, L. & Orozco, E. (2004). *Acta Cryst.* C**60**, i14–i16.

Kim, K. N., Jung, H. K., Park, H. D. & Kim, D. (2002). *J. Lumin.* **99**, 169–173.

Klein, C.(1989). *Minerals and Rocks, Exercises in Crystallography, Mineralogy and Hand Specimen Petrology*, p. 20. New York: John Wiley and Sons.

Lara, J. A., Riveros, H. G., Reyes-Gasga, J. & Yacamán, M. J. (1991). *J. Crystal Growth*, **109**, 137–141.

Morniroli, J. P. & Steeds, J. W. (1992). *Ultramicroscopy*, **45**, 219–239.

Pattison, P., Knudsen, K. D., Cerny, R. & Koller, E. (2000). *J. Synchrotron Rad.* **7**, 251–256.

Rao, C. N. R., Vanitha, P. V. & Cheetham, A. K. (2003). *Chem. Eur. J.* **9**, 828–836.

Schäfer, H. (1964). *Chemical Transport Reaction.* New York/London: Academic Press.

Taviot-Guého, C., Giaquinta, D., Palvadeau, P. & Rouxel, J. (1995). *J. Solid State Chem.* **120**, 7–11.

Taviot-Guého, C., Léone, P., Palvadeau, P. & Reuxel, J. (1999). *J. Solid State Chem.* **143**, 145–150.

Vijaya Sarathy, K., Vanitha, P. V., Ram Seshadri, A. K. & Rao, C. N. R. (2001). *Chem. Mater.* **13**, 787–795.

Wan, Z., Liu, Y., Fu, Z., Li, Y., Cheng, T., Li, F. & Fan, H. (2003). *Z. Kristallogr.* **218**, 308–315.